JOC The Journal of Organic Chemistry

Article

pubs.acs.org/joc

Designing Conical Intersections for Light-Driven Single Molecule Rotary Motors: From Precessional to Axial Motion

Michael Filatov*[,†] and Massimo Olivucci*[,‡,§]

[†]Institut für Physikalische und Theoretische Chemie, Universität Bonn, Beringstrasse 4, D-53115 Bonn, Germany

[‡]Dipartimento di Chimica, Università di Siena, Siena, Italy

[§]Department of Chemistry, Bowling Green State University, Bowling Green, Ohio 43403, United States

Supporting Information

ABSTRACT: In the past, the design of light-driven single molecule rotary motors has been mainly guided by the modification of their ground-state conformational properties. Further progress in this field is thus likely to be achieved through a detailed understanding of light-induced dynamics of the system and the ways of modulating it by introducing chemical modifications. In the present theoretical work, the analysis of model organic chromophores and synthesized rotary motors is used for rationalizing the effect of electron-withdrawing heteroatoms (such as a cationic nitrogen) on the topography and branching plane of mechanistically relevant conical intersections. Such an analysis reveals how the character of rotary motion could be changed from a precessional motion to an axial rotational motion. These concepts are then used to design and build quantum chemical models of three distinct types of Schiff base rotary motors. One of these models, featuring the synthetically viable indanylidenepyrroline framework, has conical intersection structures consistent with an axial rotation not hindered by ground-state conformational barriers. It is expected that this type of motor should be capable of funneling the photon energy into specific rotary modes, thus achieving photoisomerization quantum efficiencies comparable to those seen in visual pigments.

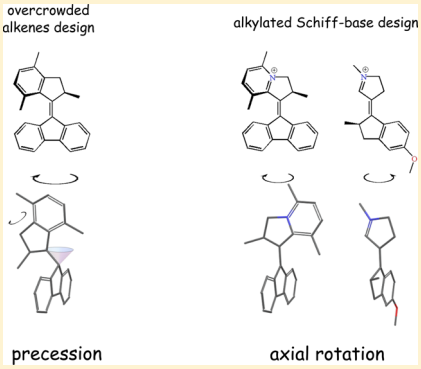

1. INTRODUCTION

Light-driven single molecule rotary motors (from now on denoted as rotary motors)[1,2] represent a class of chiral compounds capable of converting light energy into mechanical motion (rotation) of one part of the molecule (the rotor) with respect to another (the stator).[3] Rotary motors are already finding application in engineering functionalized surfaces,[4] light-controlled catalysis,[5] and building proof-of-concept nanocars.[6] The rational design of light-driven rotary motors, however, implies a thorough mechanistic understanding of the rotary process. This is based on sequential and periodic repetition of double bond photoisomerization and thermal conformational relaxation steps, which lead to a unidirectional rotation of the rotor with respect to the stator.[1,2,7−9] The thermochemical aspects of the process are well understood, and on this basis, it has been possible to increase the speed of rotation by chemical modification.[1,2] However, the ways to modulate and control the dynamics of unidirectional rotation still remain poorly understood.

Recently, the mechanistic aspects of the photoisomerization of rotary motors based on overcrowded alkenes have been investigated by nonadiabatic molecular dynamics simulations[7,8] and by ultrafast fluorescence upconversion measurements[9] establishing that conical intersections (CIs) between the ground (S_0) and the lowest excited (S_1) singlet state play a dominant role for the photodynamics. Despite a wide recognition of CIs as the most important mechanistic entity in singlet-state photochemistry,[10−14] the ways of modulating their geometric and energetic parameters by purely chemical means are not yet fully grasped. In particular, it has been found that, for the motor synthesized by Pollard et al.,[2] the CI occurring along the double bond torsion pathway requires substantial pyramidalization distortion of one of the carbon atoms and this has an impact on the motor trajectory.[7,8] As we will discuss below, the necessity to impose a pyramidalization in addition to the reactive displacement of atoms (double bond torsion) is responsible for a bicircular hippopede-type precessional motion which may be associated with the observed modest quantum yields of photoisomerization.[7−9,15]

It is the primary goal of the present work to investigate the factors influencing CI's energy and geometry with the purpose of deriving prescriptions that would enable synthetic chemists to optimize the rotary process. Below we will focus on the effect of electron-withdrawing and -donating substituents and heteroatoms introduced in the motor backbone. In addition to the induced CI energy and geometry changes, we will devote special attention to the modification of the branching plane vectors in order to redesign the directions of exiting the CI upon decay. Such an investigation will be carried out with the use of density functional calculations employing a novel, but

Received: February 21, 2014
Published: March 27, 2014

   dx.doi.org/10.1021/jo5004289 | J. Org. Chem. 2014, 79, 3587−3600

Scheme 1. Schematic Representation of Conical Intersection for Isomerization about the Double Bond

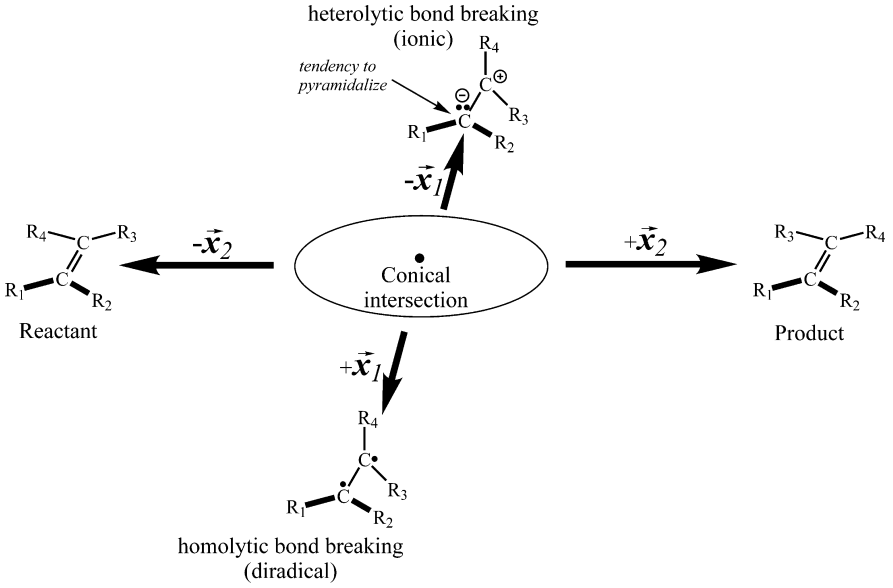

benchmarked, method enabling one to describe S_1 potential energy surfaces (PESs) and CIs in large organic molecules.[16,17]

2. CONICAL INTERSECTIONS AND THEIR BRANCHING PLANE VECTORS

CI's are points belonging to a manifold of molecular geometries at which Born−Oppenheimer PES's of two electronic states that have the same space and spin symmetry become degenerate.[18−20] For two adiabatic electronic states, which are obtained as solutions of the 2 × 2 secular problem with the Hamiltonian 1

$$\begin{vmatrix} E_I & H_{IJ} \\ H_{IJ} & E_J \end{vmatrix} \tag{1}$$

in terms of the (arbitrarily chosen, orthogonal) diabatic states I and J, such a degeneracy occurs provided that the conditions in eq 2 are fulfilled

$$E_I - E_J = 0 \tag{2a}$$

$$\langle I|\hat{H}|J\rangle = \langle J|\hat{H}|I\rangle = 0 \tag{2b}$$

where E_I and E_J are the energies of the two diabatic states and $\hat{H}$ is the electronic Hamiltonian.[10,21,22] Since these conditions are fulfilled in an N-2-dimensional subspace of the space spanned by the N internal molecular coordinates,[18−20] the CIs occur in molecules with three or more atoms. Accordingly, at any CI point the energy degeneracy is lifted along two specific coordinates defined by the gradients of the conditions in eq 2,[10,11,18−23] cf. eq 3

$$\mathbf{x}_1 = \nabla(E_I - E_J) \tag{3a}$$

$$\mathbf{x}_2 = \nabla\langle I|\hat{H}|J\rangle = \nabla H_{IJ} \tag{3b}$$

where ∇ corresponds to differentiation with respect to all nuclear coordinates. As, in the vicinity of the crossing point, the energies of the adiabatic states depend linearly on the displacement along the $\mathbf{x}_1$ and $\mathbf{x}_2$ vectors, the PESs near each CI point have the topography of a double cone.[18,21] The two vectors $\mathbf{x}_1$ and $\mathbf{x}_2$ define the branching plane (BP; sometimes also called the (g,h) plane) of a CI. Generally, the BP vectors $\mathbf{x}_1$ and $\mathbf{x}_2$ can be defined via both the diabatic electronic states (as in eq 3) as well as the adiabatic electronic states.[10,21,22]

BP vectors play an important role for the mechanism of photochemical reactions.[11,12,14,23] As we are interested in the singlet-state photoisomerization of alkenes (*cis*/*trans* or, more generally, *E*/*Z* isomerization), we shall limit the discussion to S_0 and S_1 states that correspond to $(\pi)^2$ and $(\pi)^1(\pi^*)^1$ electronic configurations of the π-bond. As was originally reported by Michl et al.,[24] the photoisomerization about a double bond in alkenes involves primarily two electronic states, which can be associated with homolytic and heterolytic bond breaking. The homolytic π-bond breaking results in a diradicaloid electronic configuration, while the heterolytic bond breaking leads to an ionic (or zwitterionic) electronic configuration. By virtue of the sign-change theorem (also known as geometric phase or Berry phase theorem),[20] a CI is to be present inside a closed path connecting the conformations that correspond to the two π-bond breaking mechanisms (see Scheme 1).[12,25] It is convenient to associate these conformations with the respective transition states on the S_0 PES.[12,25] Note, however, that such transition states may not always be located on the S_0 PES and one may speak about a hypothetical transition state that possesses the respective electronic structure (diradical or ionic).[25]

Let us assume a nuclear movement along the direction of the $\mathbf{x}_1$ vector while keeping the interstate coupling matrix element H_{IJ} at zero. For such a movement, when passing through the CI point, the S_0 (or S_1) wave function experiences a sudden switch from diradical to ionic (or vice versa). It is therefore natural to assume that such a movement is aligned with a path connecting the two transition states (hypothetical or real), TS_{dir} (transition state with diradical character) and TS_{ct} (transition state with charge transfer (ionic) character), see also Scheme 1.[12] Consistently, a movement along the direction of the $\mathbf{x}_2$ vector (while keeping the energy difference $E_I - E_J$ at zero) should contain a twist about the double bond.[12] Indeed, breaking of the π-component of the double bond in the ground electronic state can be achieved by twisting motion which brings the two fragments, $-(R_1)C(R_2)-$ and $-(R_3)C(R_4)-$, into approx-

dx.doi.org/10.1021/jo5004289 | J. Org. Chem. 2014, 79, 3587−3600

Scheme 2. Schematic Representation of CIs for the Situations Where the π-Bond Breaking Is Dominated by a Homolytic Mechanism (A) or Heterolytic Mechanism (C) and Where Both Mechanisms Are Approximately Equienergetic (B)[a]

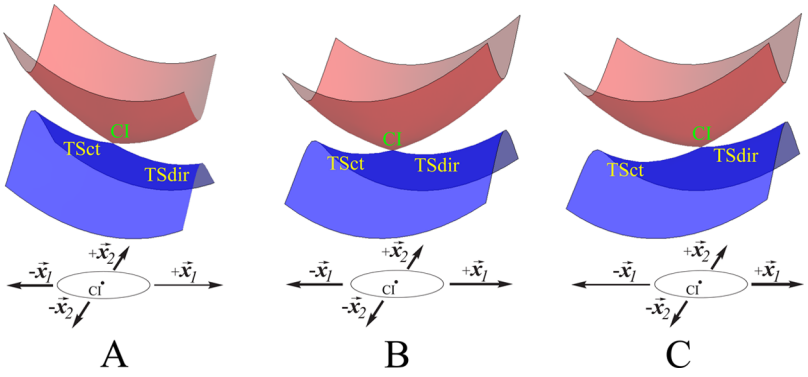

[a]To make the CI point more visible, the branching plane is rotated through 90° with respect to Scheme 1.

imately orthogonal orientation. In such a conformation, the interaction between the fragment wave functions is minimal, and this leads to vanishing H_{IJ} at the CI point.[12] Note, however, that individual orientation of the $\mathbf{x}_1$ and $\mathbf{x}_2$ vectors is not unique, and these vectors may be rigidly rotated with respect to those shown in Scheme 1.[21] Such a rotation however leaves the BP orientation unchanged.

The topography and the location of the CI can be related to the relative stability of TS_{dir} and TS_{ct}.[25,26] This is illustrated in Scheme 2, where the S_0 and S_1 PES's are shown for the cases of predominant homolytic π-bond breaking (panel A), approximately equienergetic homolytic and heterolytic bond breaking mechanisms (panel B), and predominant heterolytic π-bond breaking mechanism (panel C). It can be hypothesized that the CI occurs energetically and geometrically in the proximity of the S_0 conformation (TS_{dir} or TS_{ct}) that corresponds to the least energetically favorable π-bond breaking mechanism.[16,17] This is supported by the results of CI optimizations (see refs 16 and 17) and by theoretical analysis (see ref 25). Thus, the geometry and energy of the CI can be modulated by changing the relative stability of TS_{dir} and TS_{ct}.

In alkenes, the homolytic π-bond-breaking mechanism is energetically more favorable than the heterolytic mechanism.[25,27] It may be even impossible to locate a transition state that corresponds to the latter mechanism.[17,25] When the π-bond electron pair is shifted toward one end of the π-bond, as in TS_{ct}, the resulting structure can be stabilized by pyramidalization (combined with a bond stretching) of the anionic carbon atom similar to carbanions (see Scheme 1).[28] As the S_1/S_0 CI in this case occurs close to TS_{ct} (see panel A in Scheme 2), this will feature similar pyramidalization distortion and one of the BP vectors ($\mathbf{x}_1$ in Scheme 1) will be aligned with nuclear motion that connects the unpyramidalized TS_{dir} geometry with the pyramidalized TS_{ct} geometry, whereas the other BP vector ($\mathbf{x}_2$ in Scheme 1) describes double bond torsion. Thus, the BP of such a CI can be described as a *twist-pyramidalization/stretching* or, for brevity, *twist-pyramidalization* plane.

In the presence of substituents or heteroatoms with a strong negative mesomeric effect, such as the cationic nitrogen (N^+) center in protonated or alkylated Schiff bases, the heterolytic breaking of the π-bond becomes favorable (see panels B, C in Scheme 2) as the lone-pair is now stabilized by the heteroatom (e. g., protonated amino group of the Schiff base) and the requirement for pronounced pyramidalization is diminished. In such a case, the CI is reached by a geometric distortion that destabilizes the TS_{ct} conformation (or possibly, both conformations, TS_{ct} and TS_{dir}) and is dominated by the *stretching* distortion alone rather than *pyramidalization/stretching* distortion as in unsubstituted hydrocarbons. In conjugated systems, such a distortion involves double bond stretching−single bond contraction displacement (alternatively, bond length alternation (BLA) displacement) as was observed in models of the retinal chromophore.[12,29,30] Hence, when electron-withdrawing substituents/heteroatoms are present, one of the BP vectors describes a nuclear motion that corresponds to the BLA displacement and the CI BP becomes a *twist-BLA* plane. In the following, we present computational results that illustrate these conjectures.

3. RESULTS AND DISCUSSION

In section 3.1, we study the BP vectors of minimum energy CIs (MECIs) in basic organic molecules. These calculations are deemed to illustrate the model presented in section 2. For these molecules, the REKS method employed in this study (see section 5) was recently benchmarked[17] against the MECI geometries available in the literature;[31,32] the latter were obtained using high-level multireference ab initio methods such as MRCI and CASPT2. This study has demonstrated that the method is capable of reproducing the reference MECI geometries with an accuracy better than 0.1 Å for the root-mean-square-deviation (RMSD) of the atomic coordinates.[17] An extended benchmarking of the REKS method performance that includes not only the MECI geometries but also the BP vectors is being currently carried out and will be published elsewhere.

In section 3.2, we instead characterize a synthetically achieved rotary motor based on a crowded alkene framework. In sections 3.3 and 3.4, we apply the REKS method (see section 5) to design rotary motors based on the replacement of an sp^2 carbon with an isoelectronic but electron-withdrawing N^+ center.

3.1. Ethylene, Styrene, and a Protonated Schiff Base.

Ethylene is a benchmark molecule often used to study the role of CIs in double-bond photoisomerization.[13,24,33−35] Its twisted-pyramidalized CI is one of the most efficient S_1 relaxation channels ever documented[13,34−37] and is the result of crossing between the diradicaloid and ionic states, which correspond to the homolytic and heterolytic π-bond breaking mechanism, respectively. As shown in the lower panel of Figure

dx.doi.org/10.1021/jo5004289 | J. Org. Chem. 2014, 79, 3587−3600

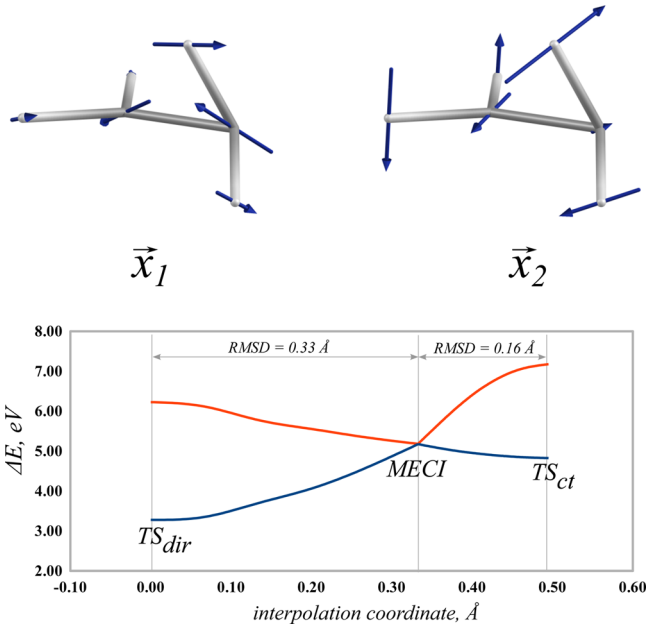

Figure 1. Upper panel: Branching plane vectors of C_2H_4 twisted-pyramidalized MECI calculated using the SI-SA-RE-BH&HLYP/6-31G* method. The MECI geometry is taken from ref 17. The BP vectors are normalized against the Frobenius norm (see the Supporting Information for further details). Lower panel: Profiles of the S_0 and S_1 PES's of ethylene obtained in a rigid scan between the TS_{dir}, MECI, and TS_{ct} geometries. Near the MECI point, the direction of atomic displacements is aligned with the direction of the $\mathbf{x}_1$ vector.

1 (see also Figure 6 of ref 17), a pyramidalization distortion applied to one of the carbon atoms leads to destabilization of the S_0 diradical state and to slight stabilization of the S_1 ionic state. Eventually, the two states become degenerate leading to the MECI point. As can be also judged by RMSD of the atomic coordinates at the MECI point from the diradicaloid TS_{dir} and ionic TS_{ct} geometries (see Figure 1 and Figures 1 and 6 in ref 17), which according to the SI-SA-RE-BH&HLYP calculations are 0.3328 and 0.1623 Å, respectively, the S_0/S_1 MECI is close to the TS_{ct} geometry, thus confirming the thesis that the CI occurs closer to the transition state (for homolytic or heterolytic π-bond breaking) which has a higher energy. From the results of ref 17, the S_0 TS_{dir} structure lies at 3.275 eV (75.5 kcal/mol) and the S_0 TS_{ct} structure at 4.823 eV (111.2 kcal/mol) above the S_0 equilibrium conformation of ethylene (the MECI occurs at 5.158 eV (118.9 kcal/mol) according to the SI-SA-RE-BH&HLYP/6-31G* calculations).[17]

As seen from Figure 1, the $\mathbf{x}_2$ vector corresponds to a twisting about the double-bond movement as was anticipated in Section 2. The $\mathbf{x}_1$ vector describes a planarization displacement of the terminal CH_2 group (coupled with a slight C−C bond stretching), and motion in the $+\mathbf{x}_1$ direction should lead from the MECI point to the TS_{dir} geometry. Motion from the MECI point in the $-\mathbf{x}_1$ direction leads to the TS_{ct} geometry, which as can be deduced from Figure 1, corresponds to a change in pyramidalization connecting the two transition states coupled with stretching of the C−C bond and also with H-transfer to another CH_2 group (see also the discussion in ref 25).

Introducing a phenyl substituent at the double bond does not appear to lead to a change in the character of the BP vectors. Indeed, the two styrene's MECIs, which feature pyramidalization of the terminal carbon atom (CI_1) and of the benzylic carbon (CI_2), have been reported in ref 17. As is apparent from Figure 2 (see also Tables 2 and 3 of the Supporting Information), for both CIs $\mathbf{x}_2$ is aligned with the twisting

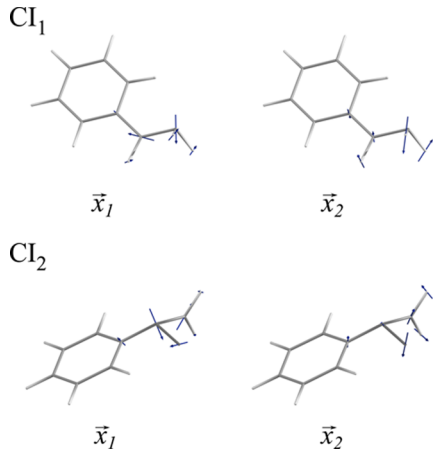

Figure 2. Branching plane vectors of CI_1 and CI_2 in styrene calculated using the SI-SA-RE-BH&HLYP/6-31G* method. The CI_1 and CI_2 geometries were taken from ref 17.

about the double bond and $\mathbf{x}_1$ with the pyramidalization/planarization of the respective carbon atom. This indicates that the aryl group has only a minor effect on the transition states describing the homolytic and heterolytic breaking of the vinyl double bond. According to ref 17, CI_1 lies 4.418 eV (101.9 kcal/mol) and CI_2 5.042 eV (116.3 kcal/mol) above the S_0 equilibrium structure of styrene. Their relative energies are insignificantly lower than the twisted-pyramidalized MECI energy of ethylene (5.158 eV), and that corresponds to a weak stabilization of the ionic configurations corresponding to the heterolytic breaking of the vinyl π-bond.

A strong electron-withdrawing heteroatomic center, such as the cationic nitrogen, has a pronounced influence on BP. Figure 3 shows the BP vectors of the MECI point of the protonated

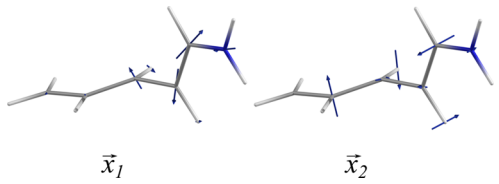

Figure 3. Branching plane vectors of PSB3MECI calculated using the SI-SA-RE-BH&HLYP/6-31G* method. The MECI geometry was taken from ref 17.

Schiff base (PSB3). The $\mathbf{x}_2$ and the $\mathbf{x}_1$ vectors of PSB3's MECI correspond to *twist-BLA* displacements; see the discussion in section 2. The N^+ center strongly stabilizes TS_{ct} for the heterolytic breaking of the π-component of the $C_3{=}C_4$ double bond, which results from electron transfer to the amine end of PSB3. Due to localization of the nitrogen lone pair, no pyramidalization is needed to stabilize TS_{ct}. Therefore, the MECI point in PSB3 is reached by double-bond stretching/single-bond contraction distortion of the ca. 90°-twisted conformation.[16,17,29] The PSB3 MECI point lies markedly lower with respect to the S_0 equilibrium structure, at 3.012 eV (69.5 kcal/mol) according to the SI-SA-RE-BH&HLYP/6-31G* calculations,[17] than the CI points in ethylene and styrene.[17]

dx.doi.org/10.1021/jo5004289 | J. Org. Chem. 2014, 79, 3587−3600

Scheme 3. Sketch of the S_0 (Blue) and S_1 (Red) Potential Energy Surfaces of the Unsubstituted Fluorene Molecular Rotary Motor along the Rotation Pathway[a]

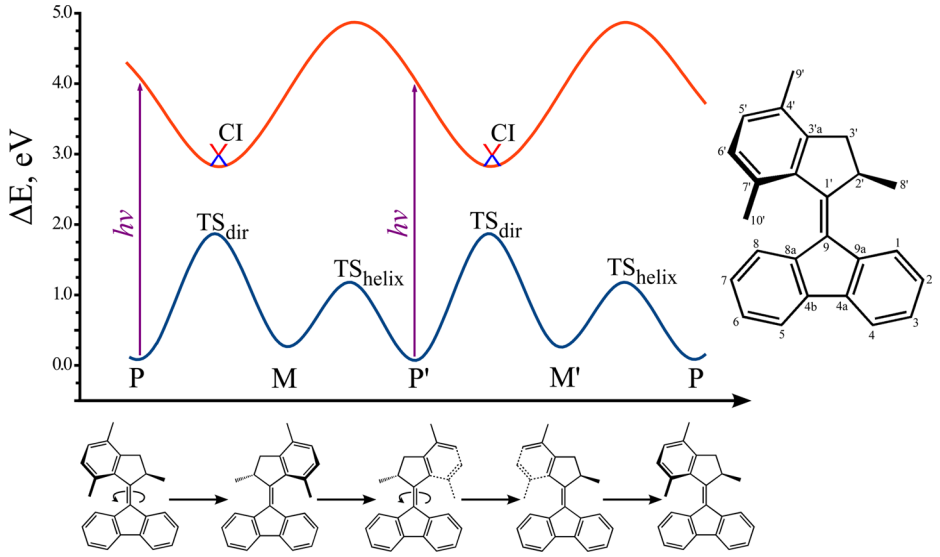

[a]The depicted sequence of transformations corresponds to a CCW rotation of the upper part with respect to the fluorene moiety. Numbering of carbon atoms is given in the inset. See refs 7 and 8 for more details.

3.2. Fluorene Light-Driven Rotary Motor. The observations made in section 3.1 are confirmed for the larger fluorene based light-driven molecular rotary motor, 9-(2,4,7-trimethyl-2,3-dihydro-1*H*-inden-1-ylidene)-9*H*-fluorene.[2,7,8] The molecular structure along with the S_0 and S_1 energy changes of this motor are schematically shown in Scheme 3 for a sequence of transformations that the motor undergoes during its operation.

To briefly remind the reader about the mode of function of the fluorene motor; the motor exists in two major chiral forms, a conformationally stable (**P**) form and a metastable (**M**) form, which according to the SI-SA-RE-BH&HLYP/6-31G* calculations lies 0.194 eV (4.5 kcal/mol) above **P**. Photoexcitation of **P** results in a rapid formation of **M**, which occurs on a time scale of 1.5 ps according to computational nonadiabatic molecular dynamics modeling[7,8] and experimental ultrafast fluorescence upconversion measurements.[9] The relaxation of the S_1 state occurs via a CI located in the vicinity of the minimum on the S_1 PES (see Scheme 3; see also Figure 3 of ref 7 and Figures 1 and 2 of ref 8). On the S_0 PES, the metastable conformer **M** relaxes via thermally activated helix inversion pathway (the respective transition state is denoted TS_{helix} in Scheme 3) to the stable conformation **P′** rotated through 180° in the CCW direction with respect to the original orientation of **P**. In the next half-loop of the motor, this sequence of transformations is repeated for **P′**. Notice that due to the fluorene symmetry, **P** and **P′** are identical.

In the present work, the geometries of the S_0 species have been optimized using the RE-BH&HLYP/6-31G* method, and the energies were subsequently calculated for the S_0 and S_1 states using the SI-SA-RE-BH&HLYP/6-31G* method. The latter energies are reported in Table 1.

As expected for a crowded alkene not containing electron-withdrawing centers, the S_1/S_0 CIs feature strong pyramidalization of the C_9 carbon atom (see Scheme 3 for the numbering) and occur at a twisted-pyramidalized geometry as shown in Figure 4 (in the previous SA-REKS study of the PESs of fluorene motor,[7] the CIs were only approximately located from the PES scans). Both MECIs optimized in the present work

Table 1. Relative Energies of the Species Shown in Scheme 3 and S_1/S_0 MECIs of Fluorene Motor[a]

	relative energies, eV (kcal/mol)	
	S_0	S_1
P	0.000 (0.0)	3.873 (89.3)
M	0.194 (4.5)	3.688 (85.0)
CI_1	2.957 (68.2)	2.957 (68.2)
CI_2	3.065 (70.7)	3.065 (70.7)
TS_{dir}	1.783 (41.1)	2.740 (63.2)
TS_{helix}	1.092 (25.2)	4.781 (110.3)

[a]For total energies, see Table 8 of the Supporting Information.

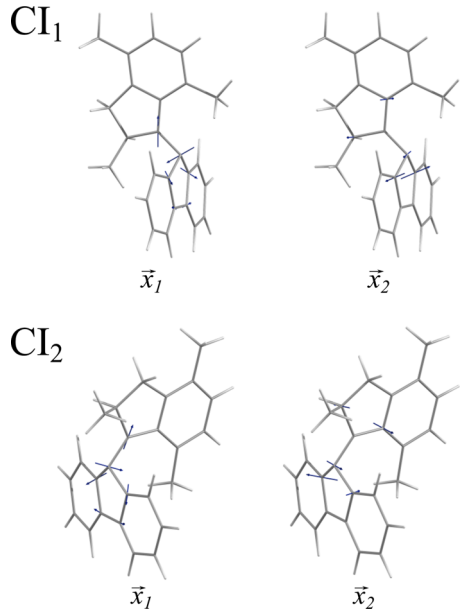

Figure 4. CIs and branching plane vectors of fluorene motor calculated using the SI-SA-RE-BH&HLYP/6-31G* method.

dx.doi.org/10.1021/jo5004289 | J. Org. Chem. 2014, 79, 3587−3600

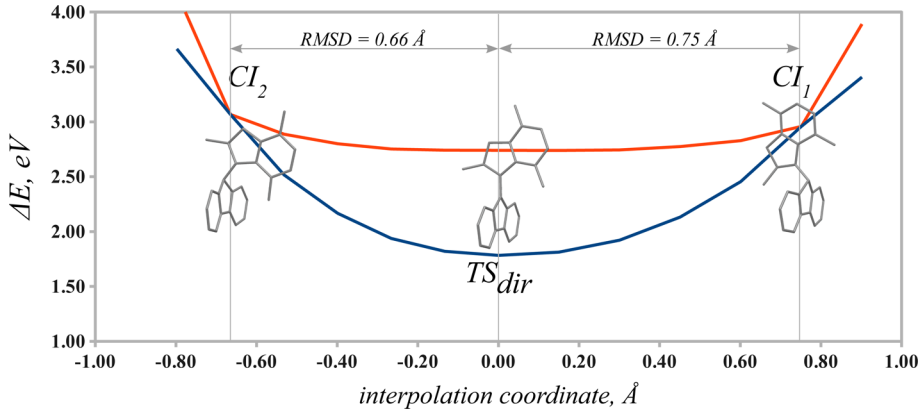

Figure 5. Profiles of S_0 and S_1 PESs of fluorene motor obtained using the SI-SA-RE-BH&HLYP/6-31G* method in a rigid scan between the respective optimized geometries. CI_1 and CI_2 geometries are strongly pyramidalized at the C_9 atom, which results in a precessional motion during the motor's operation.

(see Tables 6 and 7 of the Supporting Information for more details), CI_1 and CI_2, differ by the direction of the tilt of the rotor part with respect to the fluorene moiety. Their BP vectors correspond to *twist-pyramidalization* motion (see Figure 4) which is typical for alkenes, such as ethylene and styrene, and also stilbene.[38] According to the SI-SA-RE-BH&HLYP S_0 and S_1 PES scans along $\mathbf{x}_1$ and $\mathbf{x}_2$ near both MECI points, both MECIs have sloped topography, and there is a substantial slope on the S_0 PES toward TS_{dir}, while a slope toward the **M** conformer is much less pronounced on the S_0 PES (see Figure 1 of the Supporting Information).

Energetically, both CIs lie ca. 0.22−0.33 eV above the S_1 energy at the TS_{dir} geometry, which corresponds to the homolytic breaking of the $C_9{=}C_{1'}$ double bond. According to refs 7 and 8, TS_{dir} occurs at a geometry near the minimum on the S_1 PES. The two CIs occur on the fringes of the S_1 minimum basin, and the profile of the S_0 and S_1 PESs in the region between the CIs and TS_{dir} is shown in Figure 5. The SI-SA-RE-BH&HLYP/6-31G* PES profiles in Figure 5 were obtained in a rigid scan using the parabolic interpolation of the atomic coordinates between the three anchors; see also ref 17.

For the fluorene motor, the homolytic breaking of the $C_9{=}C_{1'}$ π-bond is considerably more favorable than the heterolytic one. Although no TS_{ct} for the latter bond-breaking mechanism could be found during the geometry optimizations, the energetic difference between the mechanisms can be roughly estimated by comparing the energies of separate fragments obtained by complete breaking of the $C_9{=}C_{1'}$ bond and saturating the dangling σ-bonds by methyl groups CH_3 (see also ref 17 for similar evaluations). The choice of the fragments is justified by considering Lewis diagrams which correspond to the homolytic and heterolytic breaking of the π-component of the central double bond as shown in Scheme 4. The total energy of the fragments $(\text{fluorene})^{\bullet} + (\text{rotor})^{\bullet}$ that corresponds to the homolytic bond breaking is 4.49 eV (103.5 kcal/mol) lower than the total energy of the ionic combination $(\text{fluorene})^{-} + (\text{rotor})^{+}$. The other ionic combination of fragments, $(\text{fluorene})^{+} + (\text{rotor})^{-}$, lies 1.91 eV (44.0 kcal/mol) above the former ionic combination and can be discarded. This comparison of the fragment energies indicates that a CI in such a motor molecule should occur considerably higher than the S_0 energy level of TS_{dir} (this is indeed the case, see Table1) and that the π-electron pair of the $C_9{=}C_{1'}$ double bond is shifted toward the fluorene moiety, as the latter has a greater

Scheme 4. Lewis Diagrams for Homolytic and Heterolytic Breaking of the Double Bond in Fluorene Motor

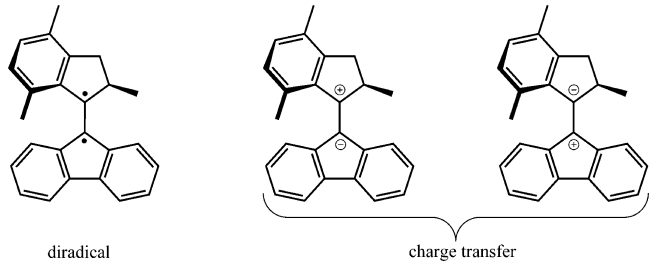

electronegativity than the rotor. This is consistent with the computed pyramidalization at the C_9 and not $C_{1'}$ atom.

The electronic structure of the S_1 state at TS_{dir} corresponds to the heterolytic breaking of the $C_9{=}C_{1'}$ π-bond and the energy of this state is slightly (by ca. 0.2 eV) raised by the pyramidalization distortion (see Figure 5). The S_0 state (which has a diradical character at the TS_{dir} geometry) does not benefit from the pyramidalization distortion and it is strongly destabilized by ca. 1.2 eV. Hence, the CI of the fluorene motor is reached due to strong pyramidalization distortion at C_9. Therefore, the motion of the rotor part of the molecule, when starting from **P**, reaching the CI, and following the progression illustrated in Scheme 3, would not represent a pure rotation about the axis of the central double bond but would be more similar to a bicircular hippopede-like precession (see Scheme 5, left) with respect to the stator axis.[7,8]

Although the pyramidalization distortion may be assisting at relieving from the steric crowding during rotation of the motor, it may lead to a reduced effectiveness of the photoisomerization. Indeed, as the CIs are located on the fringes of the S_1 minimum, it is less likely that they can be reached by the wavepacket represented by a swarm of trajectories initiated at the Franck-Condon (FC) point of **P**. This swarm of trajectories may be funneled toward the S_1 minimum (approximately at the TS_{dir} geometry) and only a relatively small fraction of the trajectories will be able to reach the CIs on first approach. This conjecture seems in line with the quantum yield of **P** → **M** photoisomerization obtained in the theoretical simulations[8] and experimental measurements.[9] Consequently, the motor may perform several torsion-pyramidalization motions while remaining on the S_1 PES before reaching a CI. Circumstantial evidence for such behavior is provided by the experimental observation

dx.doi.org/10.1021/jo5004289 | J. Org. Chem. 2014, 79, 3587−3600

Scheme 5. Left Panel: Bicircular Precessional-Type Motion (Hippopede) of the Head of the Rotating Axle of the Rotor (Dashed Line) on the Plane Orthogonal to the Stator Axis (Represented by a Blue Bold Line) Discussed for the Fluorene Motor.[a] Right Panel: Axial Motion Discussed for Motors 1, 2, and 4

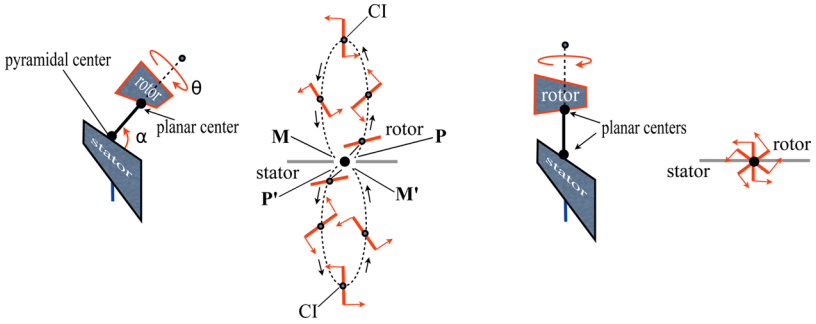

[a]Consistent with the CI structures of Figure 4, the swinging angle α appears to be roughly proportional to sin θ.

of a low frequency (ca. 110 cm^{-1}) modulation of the residual fluorescence intensity of fluorene motor,[9] which was interpreted as following from swinging of the nuclear wavepacket on the S_1 PES between the FC points (optically bright) and the S_1 minimum (optically dim).[9] As conversion of the energy of light to rotary mechanical motion occurs during the photoisomerization stage (and not the thermal relaxation step), it seems desirable to eliminate the necessity for pyramidalization distortion.

3.3. Light-Driven Rotary Motors Containing an Electron-Withdrawing N^+ Center. To remove the need for pyramidalization at a MECI it is necessary to introduce a strong electron-withdrawing center in the rotor framework. Such an effect is achieved, for example, in PSB3 which has a purely twisted geometry at the S_1/S_0 CI and a *torsion-BLA* motion in its branching plane.[29] It is therefore plausible that introducing an N^+ center in the backbone of the rotor part would remove the need for pyramidalization to reach a CI and result in a motor molecule that would be capable of performing (nearly) pure rotation about the central double bond (see Scheme 5, right). As we will discuss below, this has actually been achieved in the laboratory through the synthesis of *N*-alkylindanylidenepyrrolinium (NAIP) systems.

In order to computationally confirm the expected effect of N^+ center on the CI and BP structures of motors homologous to the fluorene motor, we begin by focusing on structures **1** and **2** in Scheme 6. In section 3.4, we will discuss the related

Scheme 6. N-Substituted Rotary Motors Studied in This Work

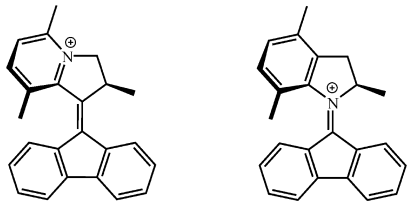

1 **2**

synthetically achieved NAIP switch **3** and the designed motor **4** (see Scheme 7). It is apparent that these compounds display functional groups related to PSB3.

A crude estimate of the energetic preference for homolytic and heterolytic breaking of the $C_9{=}C_{1'}$ bond (see Scheme 8) based on the fragment energies reveals that the heterolytic π-bond breaking mechanism becomes much more favorable as compared to the fluorene motor. In particular for the motor **1**, the total energy of the $(\text{fluorene})^{\bullet}$ + $(\text{rotor})^{+\bullet}$ fragments (homolytic bond breaking) is only 0.89 eV (20.7 kcal/mol) lower than the energy of the $(\text{fluorene})^{+}$ + (rotor) fragments (heterolytic bond breaking). Thus, the substitution in **1** results in a considerable reduction of the energy gap between the homolytic and heterolytic $C_9{=}C_{1'}$ bond breaking mechanisms and may potentially lead to a S_1/S_0 CI that has lower energy than in the fluorene motor. A similar fragment analysis for the motor **2** reveals that the heterolytic π-bond breaking mechanism becomes slightly more favorable by a mere 0.14 eV (3.1 kcal/mol).

Scheme 7. Synthetic N-Alkylated Indanylidene Pyrroline (NAIP) Molecular Switch (3) and Rotary Motor (4)[a]

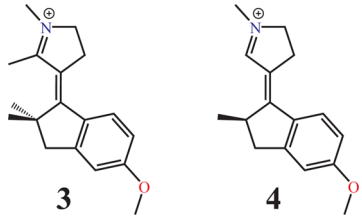

3 **4**

[a]For both species, the *E*-conformer is shown.

Scheme 8. Lewis Diagrams for Homolytic and Heterolytic Breaking of the Double Bond in 1, 2, and 4

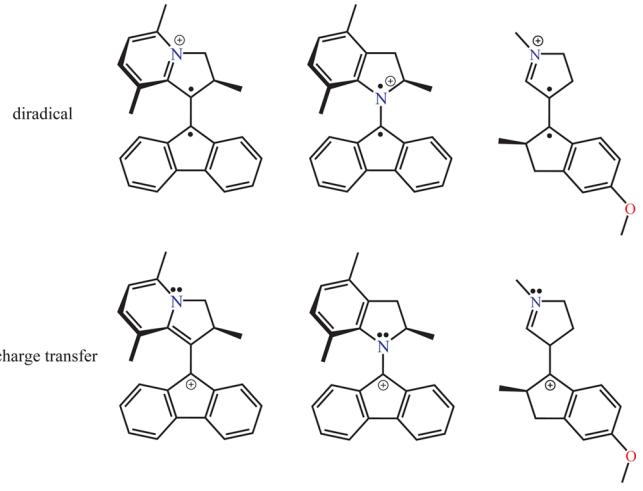

dx.doi.org/10.1021/jo5004289 | J. Org. Chem. 2014, 79, 3587−3600

The relative energies of the FC points, metastable conformations, as well as the energies of TSs and MECIs of the two motors (see Scheme 3 for reference) calculated using the SI-SA-RE-BH&HLYP/6-31G* method are collected in Table 2. For **1**, a S_0 TS_{ct} structure could not be located, and only TS_{dir} was found on the S_0 PES using the RE-BH&HLYP/6-31G* geometry optimization. For **2**, both transition states TS_{dir} and TS_{ct} were located on the S_0 PES. The reason why TS_{ct} could not be located for **1** is most likely due to the fact that such a transition state, if present, would be located extremely close to the S_1/S_0 CI that is located 0.375 eV above TS_{dir} on the S_0 PES. The shape of the S_0 and S_1 PESs of **1** and **2** along a direction connecting MECI and TS_{dir} or TS_{ct} is shown in Figure 6. As seen from Figure 6, the MECI geometry for both motors does not feature noticeable pyramidalization. Furthermore, for both motors, MECI occurs in a proximity of the TS_{dir} geometry that corresponds to a pure twist about the central double bond. This can be judged from the RMSD of atomic coordinates at the MECI geometry from the TS_{dir} geometry which is reduced by a factor of 3 as compared to the fluorene motor; see Figure 5. Note that the shape of the S_0 PES of **1** in Figure 6 does indeed indicate that a TS_{ct} might have occurred almost at the position of MECI.

Table 2. Relative Energies of the Thermally Stable and Metastable Conformers, Ground-State TSs, and S_0/S_1 MECI of Molecular Motors 1 and 2[a]

	relative energies, eV (kcal/mol)	
	S_0	S_1
	molecular motor **1**	
1-P	0.000 (0.0)	3.344 (77.1)
1-M	0.133 (3.1)	3.210 (74.0)
MECI	2.004 (46.2)	2.005 (46.2)
TS_{dir}	1.629 (37.6)	2.190 (50.5)
TS_{helix}	1.085 (25.0)	4.011 (92.5)
	molecular motor **2**	
2-P	0.000 (0.0)	2.736 (63.1)
2-M	0.182 (4.2)	2.772 (63.9)
MECI	1.768 (40.8)	1.769 (40.8)
TS_{dir}	1.689 (39.0)	1.898 (43.8)
TS_{ct}	1.411 (32.5)	2.294 (52.9)
TS_{helix}	1.227 (28.3)	3.635 (83.8)

[a]For total energies, see Tables 11 and 14 of the Supporting Information.

A more accurate view of the **1** and **2** MECIs is shown in Figure 7 along with the corresponding BP vectors. Figure 7 shows not only that **1** and **2** do not feature pyramidalization but also that the character of the BP is changed from *twist-pyramidalization* (as in fluorene motor) to *twist-BLA* (as in PSB3).

Both MECIs have a weakly sloped topography (see S_0 and S_1 PES scans near MECI points in Figure 2 of the Supporting Information), and there is a substantial slope on the S_0 PES

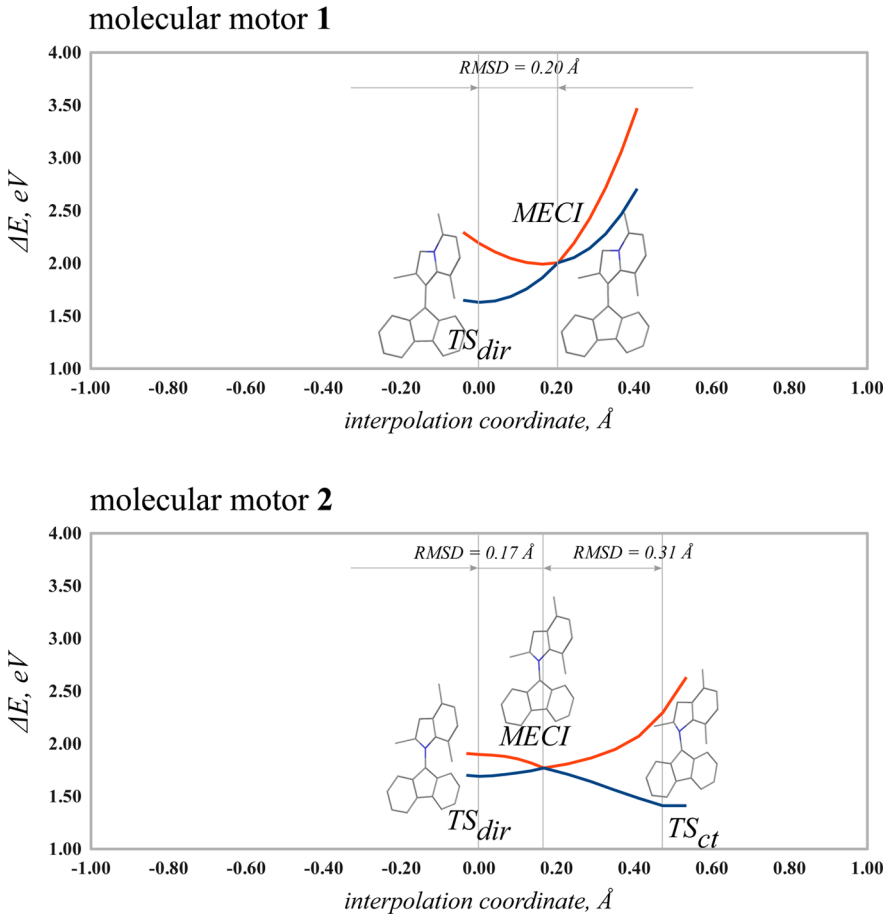

Figure 6. Profiles of S_0 and S_1 PESs of molecular motors **1** (upper panel) and **2** (lower panel) obtained using the SI-SA-RE-BH&HLYP/6-31G* method in a rigid scan between the respective optimized geometries.

dx.doi.org/10.1021/jo5004289 | J. Org. Chem. 2014, 79, 3587−3600

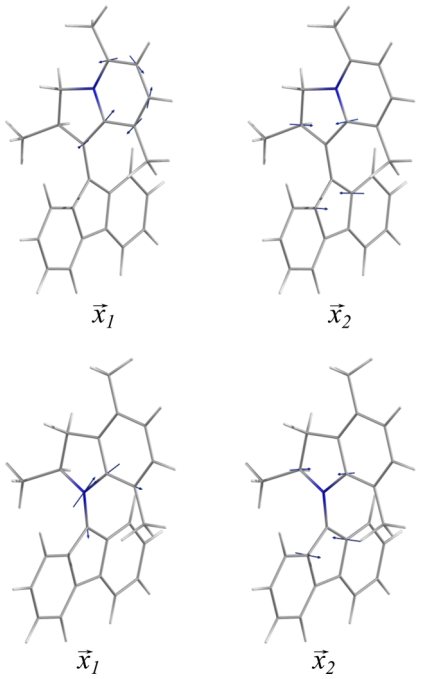

Figure 7. MECIs and branching plane vectors of molecular motors **1** (upper panel) and **2** (lower panel) calculated using the SI-SA-RE-BH&HLYP/6-31G* method.

toward TS_{dir} (for **1**) or TS_{ct} (for **2**). It is therefore expected that, when exiting the strong nonadiabatic coupling region near the CI, the mode corresponding to the BLA displacement of atomic coordinates will be excited in **1** and **2** and not the pyramidalization mode. Furthermore, as seen from Figure 6 (see also Figure 2 of the Supporting Information), the MECI points of **1** and **2** are located at the minimum on the S_1 PES of the two motors and there should be a high probability of intercepting the MECI points (or, better to put it, CI seams) by the nuclear trajectories started at the respective FC points as they propagate down the drain on the S_1 PES.

A closer look at the data in Figure 2 reveals that, for **2**, the S_0 isomerization about the double bond proceeds most likely via TS_{ct} which lies 0.279 eV (6.4 kcal/mol) lower than the respective TS_{dir} structure. Furthermore, the TS_{helix} structure for the thermal helix inversion **2M′** → **2P′** is only 0.184 eV (4.2 kcal/mol) lower than TS_{ct} in **2** thus making this motor less suitable for practical implementation as it will have an increased probability for faulty operation (going backward via thermal pathway on the S_0 PES). The motor **1**, however, has TS_{dir} 0.544 eV (12.5 kcal/mol) higher than TS_{helix}, thus eliminating a possibility of faulty operation by thermal backward isomerization. It is therefore a plausible candidacy for synthetic implementation of a molecular motor with improved operational efficiency.

3.4. NAIP Light-Driven Rotary Motor. The laboratory preparation of systems similar to **1** and **2** has actually been carried out in the past yielding a series of compounds related to **3** (see Scheme 7) that in the literature has been sometimes called MeO-NAIP.[39,40] Compound **3** is not a motor as it lacks the required chirality. It is therefore a light-driven molecular switch, as light of different wavelengths can be used to convert its *Z* form into the *E* form. In spite of this lack of chirality, the mentioned interconversion has been extensively investigated both computationally and experimentally and the S_1 as well as S_0 relaxation dynamics of the system are currently well understood.[39] Furthermore, the Z → *E* and *E* → *Z* quantum yields have been determined. Semiclassical trajectory simulations for MeO-NAIP[39,41] and related systems in methanol solution confirm that the S_1 relaxation involves very little pyramidalization motion. On the other hand, the same data display a clear initial acceleration along the BLA mode (one of the BP modes) followed by a slower evolution along the central double bond twisting coupled with ring out-of-plane deformations. The computed and observed excited state dynamics has a ca. 200 fs time scale, while the hot photoproduct appears after an additional 150 fs for both the *Z*- and *E*-forms. The experimentally measured quantum yield for the *Z* → *E* and *E* → *Z* isomerization process is in the range of 0.20−0.35.[39,41−43]

A chiral derivative of **3** (i.e., MeO-NAIP) can be easily designed by removal of a single methyl group from the indanylidene stator. Furthermore, in order to decrease the steric hindrance, which could impair the rotary motion, the methyl group in the heteroallylic position in the rotor may be also removed. These modifications yield the chiral NAIP **4**. Compound **4** has thus all the features of a rotary motor undergoing an axial rather then precessional rotation. In order to characterize its photocycle we have optimized the corresponding *E* and *Z* S_0 equilibrium geometries which, for the chosen enantiomer, display P helicity (**4-E** (P) FC and **4-Z** (P′) FC in Table 3), and the corresponding MECI and TS_{ct} geometries. Fragment analysis similar to motors **1** and **2** reveals that the homolytic bond breaking for compound **4** is less favorable by 0.933 eV (21.5 kcal/mol) than the heterolytic bond breaking. Hence, no TS_{dir} on the S_0 PES of **4** could be found. We also searched for the thermally unstable **M** conformers and the corresponding TS_{helix}'s, however, as shown in Scheme 9, only one structure near the **4-Z** species could be located. The **4-Z-M** form is separated from the **4-Z-P** by a barrier of only 0.1 kcal/mol, which indicates that **4-Z-M** is transient species and that the photoisomerization of **4-E-P** leads directly to **4-Z-P**, and no thermal step is necessary along this part of the cycle. Consequently, **4** should be capable of performing a low-temperature rotation as both **P** and **P′** conformers may be reached directly without passing through metastable **M** conformers.

Table 3. Relative Energies of the FC Points, Metastable Species, Ground-State TSs, and S_0/S_1 MECIs of NAIP Molecular Motor 4

	relative energies, eV (kcal/mol)	
	S_0	S_1
4-E (P) FC	0.000 (0.0)	3.349 (77.3)
4-Z (P′) FC	0.102 (2.3)	3.344 (77.1)
4-Z (M)	0.184 (4.2)	3.411 (78.6)
TS_{helix}-Z	0.187 (4.3)	3.392 (78.2)
TS_{ct}-E-Z	1.487 (34.3)	3.199 (73.8)
TS_{ct}-Z-E	1.477 (34.0)	3.199 (73.8)
MECI-E-Z	3.128 (72.1)	3.128 (72.1)
MECI-Z-E	3.128 (72.1)	3.128 (72.1)

Analysis of the energy profiles along the BLA coordinate in Figure 8 indicates a similarity with the energy profiles of the basic PSB3 chromophore. However, the range of BLA values appears wider most probably due to the delocalization of the radical and cationic centers on the conjugated phenyl ring. It

dx.doi.org/10.1021/jo5004289 | J. Org. Chem. 2014, 79, 3587−3600

Scheme 9. Schematic Comparison between the Rotation Cycle of the Fluorene Motor of Scheme 3 and Motor 4[a]

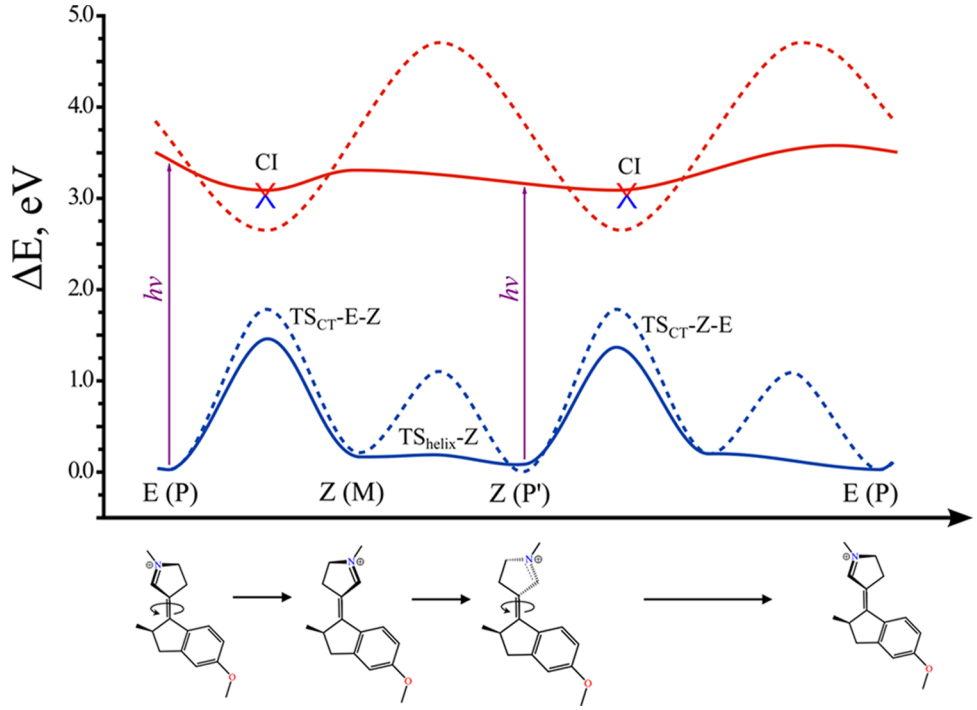

[a]The full lines represent the S_0 (blue) and S_1 (red) energy profiles (see Table 3) along the rotary motion of motor **4**. The corresponding energy profiles for the fluorene motor (see Table 1) are given as dashed lines. The depicted sequence of transformations correspond to a full CCW rotation of the rotor of **4** with respect to its indan stator.

may therefore be anticipated that the S_1 dynamics will feature an increased lifetime. It is also noteworthy that the difference in geometries between the MECI and the S_1 minima along the S_1 profile in Figure 8 is shorter in **4** than in **1** and **2** suggesting that **4** should have somewhat shorter S_1 state lifetime. Finally, from Figure 9 it is apparent that the BP vectors of **4** do not display pyramidalization contributions. It is therefore concluded that the light-driven rotary motion in **4** will be exclusively axial.

4. CONCLUSIONS

Following the notion that a singlet ultrafast photochemical reaction requires decay at a specific CI, we focus on CI energies, structures, and BPs to collect information on the photochemical reaction path and the associated dynamics. Accordingly we have investigated CIs and BPs in different light-driven rotary motors with the purpose of understanding the geometry changes occurring during the rotary cycle. Similar to transition states, where the associated transition vectors serve as guidance for designing optimal reactants to facilitate the reaction,[44] the BP of mechanistically relevant CIs should provide information useful to achieve optimal light-driven steps. On the basis of density functional REKS and SI-SA-REKS calculations, we showed that the S_1/S_0 CIs of a fluorene based rotary motor[2] feature twist about the central double bond (the rotation axis) combined with a strong pyramidalization distortion of the fluorene stator. The BP vectors of this motor mainly correspond to twisting and pyramidalization (slightly coupled with bond stretching) motion suggesting that, upon exiting the nonadiabatic coupling region, the motor molecule should have a substantial degree of excitation of the modes that correspond to pyramidalization. Besides resulting in a pronounced precession of the rotation (and isomerization) axis,[8,9] the pyramidalization required to reach the CI (or CI seam) may have an impact on the quantum efficiency (quantum yield) of the light-driven rotation steps that is currently difficult to establish.

For double-bond photoisomerization, the S_1/S_0 conical intersection occurs as a result of crossing between the electronic states which have predominantly diradicaloid character and predominantly ionic character.[12,24,25] Varying the relative stability of these electronic states by introducing electron-withdrawing or electron-donating substituents or heteroatoms gives a handle on controlling the CI structure and its BP. Indeed, we have demonstrated computationally that the character of the S_1/S_0 conical intersections can be changed from twist-pyramidalization to twist-BLA by introducing an electron-withdrawing heteroatom such as a cationic nitrogen into the rotor part of the motor. The resulting alkylated Schiff base type rotary motor **1**, Scheme 6, should thus be capable of performing a pure axial rotation (in the mechanical sense) about the central double bond during its photoisomerization. As the S_1/S_0 MECI point of this motor is located at the minimum on the S_1 PES and is easily accessible by the nuclear trajectories started at the FC point, it is expected that **1** and analogous systems should have increased quantum efficiency of photoisomerization. This expectation is supported by the experimental measurements and computational investigation of the biomimetic molecular switches of the *N*-alkylated indanylidene pyrroline (NAIP) Schiff base class (e.g., structure **3**).[40−43] The currently synthesized and spectroscopically investigated NAIP switches show considerably shorter excited-state lifetimes (ca. 380−500 fs) as compared to all hydrocarbon fluorene rotary motor (ca. 1500 fs) and increased photoisomerization quantum yields, ca. 0.35[42,43] vs 0.14[9] for fluorene motor. It is therefore plausible that with suitable

dx.doi.org/10.1021/jo5004289 | J. Org. Chem. 2014, 79, 3587−3600

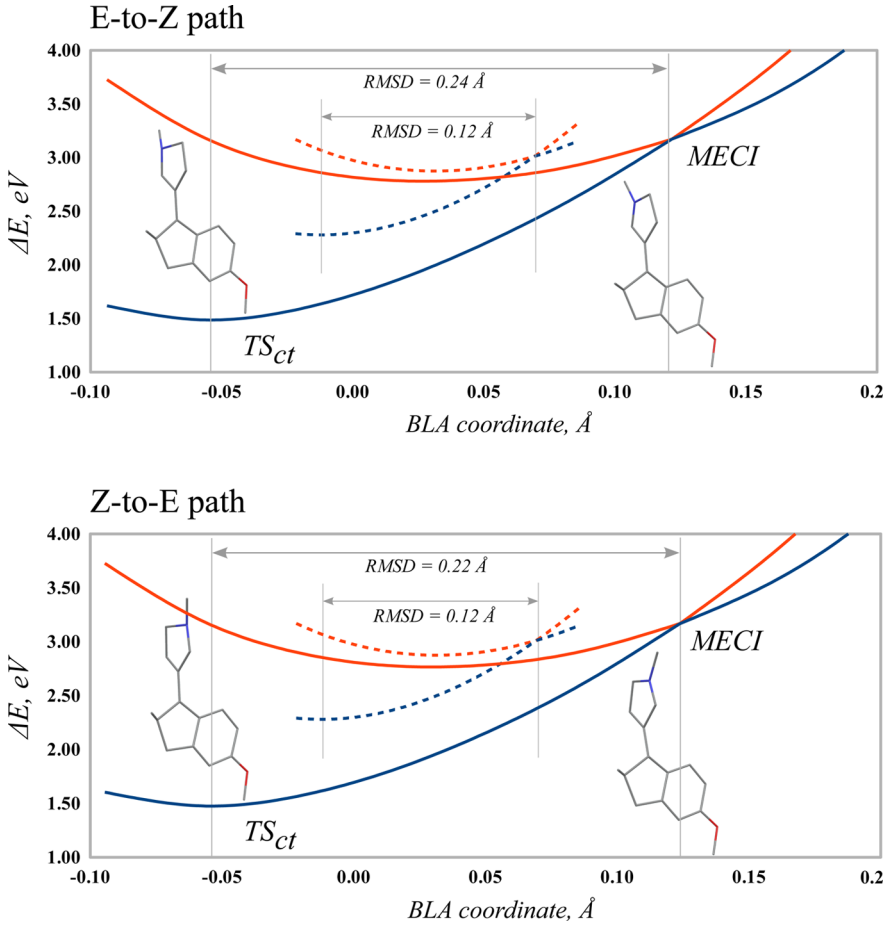

Figure 8. Profiles of S_0 and S_1 PESs of NAIP molecular motor **4** obtained using the SI-SA-RE-BH&HLYP/6-31G* method in a rigid scan between TS_{ct}-E-Z and MECI-E-Z (upper panel) and TS_{ct}-Z-E and MECI-Z-E (lower panel). For comparison, the PES profiles of PSB3 are shown as dashed curves.

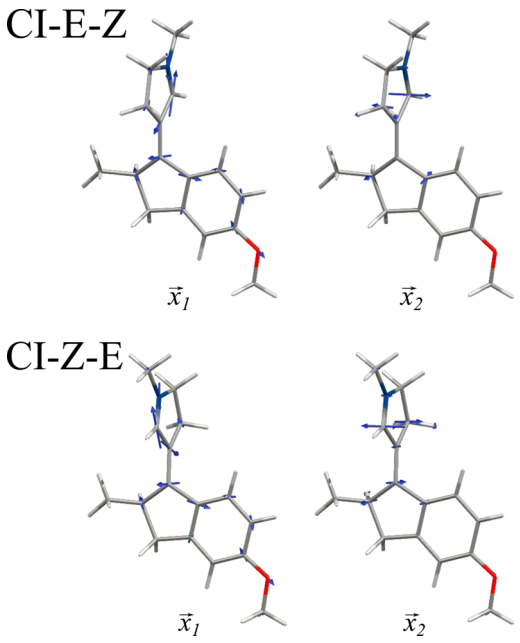

Figure 9. Geometries and branching plane vectors of molecular motor **4** MECI-E-Z (upper panel) and MECI-Z-E (lower panel) calculated using the SI-SA-RE-BH&HLYP/6-31G* method.

structural modifications the high efficiency of rhodopsin (ca. 0.66) can be reached by synthetic molecular devices.

For this reason we have designed and computationally investigated compound **4**. This compound not only shows the expected *twist-BLA* branching plane associated with an axial rotary motion but also possesses favorable S_0 features. In particular, we have provided evidence for the absence of an energy barrier controlling the **M** to **P** conformational transition occurring upon S_0 relaxation. Accordingly, motors of the type of compound **4** may efficiently funnel the photon energy into the rotary mode and ultimately, achieve maximum rotatory speed even at a low temperature.

5. COMPUTATIONAL METHODOLOGY

Because the molecules that we want to study are too large to be systematically investigated using multireference *ab initio* wave function methods accounting for dynamic electron correlation such as multireference configuration interaction (MRCI)[45] or complete active space second-order perturbation theory (CASPT2),[46] we employed a method based on density functional theory (DFT) and designed to describe electronic states of molecular systems typified by strong nondynamic electron correlation. The spin-restricted ensemble referenced Kohn−Sham (REKS) method[47−49] uses ensemble representation for the Kohn−Sham (KS) reference state[50,51] to describe the nondynamic electron correlation in the context of KS DFT.[52−55] As follows from numeric simulations in which the exact KS potential was obtained from the (known) exact density,[52,53,55] only a few individual KS determinants are sufficient to faithfully represent the

dx.doi.org/10.1021/jo5004289 | J. Org. Chem. 2014, 79, 3587−3600

density of a strongly correlated atomic or molecular system in the framework of ensemble formalism. The ensemble representation for the density leads to fractional occupation numbers of a few frontier KS orbitals.[52,53,55,56] In the case of a molecule undergoing isomerization about the double bond, which is of relevance for the current work, the doubly occupied bonding, π, and the empty antibonding, π^*, frontier orbitals become degenerate at ca. 90°-twisted conformation and a strong nondynamic correlation ensues.[27] For such a system, the REKS ground-state density and ground-state energy are represented as in eqs 4 and 5, respectively

$$\rho^{\mathrm{REKS}(2,2)}(\mathbf{r}) = \sum_{k}^{\mathrm{core}} 2\,|\varphi_k(\mathbf{r})|^2 + n_a\,|\varphi_a(\mathbf{r})|^2 + n_b\,|\varphi_b(\mathbf{r})|^2 \tag{4}$$

$$E^{\mathrm{REKS}(2,2)} = \frac{n_a}{2}E[...\varphi_a\bar{\varphi}_a] + \frac{n_b}{2}E[...\varphi_b\bar{\varphi}_b] + f(n_a, n_b)E[...\varphi_a\varphi_b] - \frac{f(n_a, n_b)}{2}E[...\varphi_a\bar{\varphi}_b] - \frac{f(n_a, n_b)}{2}E[...\bar{\varphi}_a\varphi_b] \tag{5}$$

where φ_a and φ_b are the frontier (active) orbitals with the fractional occupation numbers (FONs) n_a and n_b, φ_k are the doubly occupied (core) orbitals, the unbarred and barred orbitals are occupied with spin-up and spin-down electrons, and $f(n_a,n_b)$ is a function of the occupation numbers that was derived in refs 47−49 based on the analysis of model multiconfigurational wave functions. The function $f(n_a,n_b)$ satisfies asymptotic conditions which guarantee the correct description of strongly correlated systems, where $n_a \approx n_b \approx 1$, as well as systems without nondynamic correlation, for which $n_a \approx 2$ and $n_b \approx 0$. The energy (5) is minimized with respect to the KS orbitals φ and the FON's of the active orbitals n_a and n_b. Since eqs 4 and 5 describe a system with two active electrons in two active orbitals, a notation REKS(2,2) is adopted by analogy with the CASSCF method.

The ground state of a homosymmetric biradical obtained by complete or partial dissociation of the π-bond can be approximated by a two-configurational wave function 6[27]

$$\Phi_0 = \sqrt{\frac{n_a}{2}}\,|...\phi_a\bar{\phi}_a\rangle - \sqrt{\frac{n_b}{2}}\,|...\phi_b\bar{\phi}_b\rangle \tag{6}$$

while its singly excited singlet state is given by an open-shell singlet (OSS) wave function 7.[27]

$$\Phi_1 = \frac{1}{\sqrt{2}}|...\phi_a\bar{\phi}_b\rangle + \frac{1}{\sqrt{2}}|...\phi_b\bar{\phi}_a\rangle \tag{7}$$

In the framework of ensemble DFT, the former state is described by the REKS(2,2) method, whereas the latter, OSS, state can be accessed by the spin-restricted open-shell KS (ROKS) method.[57−59] As the direct calculation of an excited state (which possesses the same spin and space symmetry as the ground state) is not formally permitted in DFT[60] and may lead to artifacts in practical calculations,[61] the excited state of the diradical is obtained via an ensemble of the ground and excited states, a variational calculation of which is legitimate in the framework of DFT.[62] In the state-averaged REKS (SA-REKS) method,[63] the energy of an ensemble of states in eq 8

$$E^{\mathrm{SA\text{-}REKS}} = C_0E_0^{\mathrm{REKS}(2,2)} + C_1E_1^{\mathrm{ROKS}},\ C_0 + C_1 = 1 \tag{8}$$

is minimized with respect to the KS orbitals, which are common for both states, and with respect to the FON's of the active orbitals in the REKS(2,2) energy. In eq 8, equal weighting factors C_0 and C_1 are employed. Having completed the KS orbitals optimization, the individual energies, $E_0^{\mathrm{REKS}(2,2)}$ and E_1^{ROKS}, are calculated using these KS orbitals.

The SA-REKS method describes the S_0 and S_1 states of a homosymmetric biradical.[27] In a heterosymmetric biradical, obtained by either chemical substitution or by an asymmetric geometric distortion of a homosymmetric biradical, the states given in eqs 6 and 7 can mix with one another and this mixing becomes important in the vicinity of conical intersections.[24] Mixing between the S_0 and S_1 states can be taken into account in the state-interaction SA-REKS (SI-SA-REKS) method[16,17] via a simple 2 × 2 secular equation, as in eq 1, in which the diagonal matrix elements are given by the $E_0^{\mathrm{REKS}(2,2)}$ and E_1^{ROKS} energies and the off-diagonal matrix element is calculated using the Lagrange multiplier W_{ab} between the SA-REKS active orbitals as in eq 9

$$H_{12} = (\sqrt{n_a} - \sqrt{n_b})W_{\mathrm{ab}} \tag{9}$$

which has been obtained in refs 16 and 17 by the application of Slater−Condon rules and the variational conditions for the SA-REKS orbitals.[47,58,59] Provided that equal weighting factors are employed in eq 8, the SA-REKS orbitals remain unaffected by the application of the state interaction procedure.[16,17] The described SI-SA-REKS method has been applied to the calculation of CIs in a number of organic molecules and models of biological chromophores for which the results of multireference ab initio calculations at the CASPT2 and MRCI level are available in the literature.[31,32]

5.1. Details of Calculations. The REKS(2,2), SA-REKS, and SI-SA-REKS calculations have been carried out using the COLOGNE2012 program,[64] where these methods are implemented. All of the calculations employ the 6-31G* basis set[65] and are carried out with the use of the BH&HLYP[66] hybrid density functional. As was demonstrated in a recent study of CIs in organic molecules,[17] the BH&HLYP functional in connection with the SI-SA-REKS methodology yields the geometries and relative energies of the CI's in the best agreement with the reference data obtained from MRCI and CASPT2 calculations. Although a relatively small 6-31G* basis set of valence double-ζ quality is used in the calculations, its use was justified in a recent study of performance of the SI-SA-REKS method[17] where it was shown that the extension to a bigger basis set (valence triple-ζ 6-311G**[65]) does not result in a significant alteration of the optimized MECI geometries.

Numeric integration in the density functional calculations employed grids comprising 75 radial points and 302 angular integration points per atom. The SCF convergence criterion of 10^{-8} for the density matrix was used in all of the calculations. The following units are employed throughout the article: all geometric parameters are given in angstroms (Å), the total energies are given in Hartree atomic units (a.u.), and the relative energies are given in electron volts (eV).

The ground-state equilibrium geometries and the transition states on the S_0 PES were optimized using the REKS(2,2) method in connection with the analytic energy gradients. For the transition states, it has been confirmed that the molecular Hessian possesses one negative eigenvalue. The Hessian has been calculated by numeric differentiation of the analytic energy gradient using a 10^{-3} Å increment for the atomic coordinates.

The geometries of conical intersections were obtained with the use of the CIOpt program.[31] The algorithm used for the CI optimization employs the penalty function approach in connection with numerically calculated gradients for the ground and excited states obtained using the SI-SA-REKS method. The BP vectors, $\mathbf{x}_1$ and $\mathbf{x}_2$, in the framework of the SI-SA-REKS method are given by eq 3, where E_I and E_J have to be replaced by $E_0^{\mathrm{REKS}(2,2)}$ and E_1^{ROKS}, respectively, and H_{IJ} is to be replaced by H_{12} from eq 9. As the analytic derivatives of the SI-SA-REKS energies with respect to the nuclear coordinates are not yet implemented, the differentiation was carried out by numeric techniques. When calculating the BP vectors, the threshold for the density matrix convergence was tightened to 10^{-10} and the atomic coordinates increment was increased to 1.5×10^{-2} Å.

■ ASSOCIATED CONTENT

Supporting Information

Cartesian coordinates, total energies, and branching plane vectors of species discussed in the text. This material is available free of charge via the Internet at http://pubs.acs.org.

■ AUTHOR INFORMATION

Corresponding Authors

*E-mail: mike.filatov@gmail.com.

*E-mail: molivuc@bgsu.edu.

Notes

The authors declare no competing financial interest.

■ ACKNOWLEDGMENTS

M.F. acknowledges financial support provided by the European Union Seventh Framework Programme (FP7/2007-2013) under the IEF grant agreement no. 326652. M.O. acknowledges funding from the Italian MIUR (PRIN 2012-2014) and EU-FP7 (Marie-Curie PIOF-GA-2012-332233) grants. The European Cooperation in Science and Technology Action CM1002 (CODECS) is also acknowledged.

■ REFERENCES

(1) (a) Koumura, N.; Zijlstra, R. W. J.; van Delden, R. A.; Harada, N.; Feringa, B. L. *Nature* **1999**, *401*, 152−155. (b) Koumura, N.; Geertsema, E. M.; van Gelder, M. B.; Meetsma, A.; Feringa, B. L. *J. Am. Chem. Soc.* **2002**, *124*, 5037−5051. (c) Pijper, D.; van Delden, R. A.; Meetsma, A.; Feringa, B. L. *J. Am. Chem. Soc.* **2005**, *127*, 17612−17613. (d) van Delden, R. A.; ter Wiel, M. K. J.; Pollard, J.; Vicario, M. M.; Koumura, N.; Feringa, B. L. *Nature* **2005**, *437*, 1337−1340. (e) Landaluce, T. F.; London, G.; Pollard, M. M.; Rudolf, P.; Feringa, B. L. *J. Org. Chem.* **2010**, *75*, 5323−5325.

(2) Pollard, M. M.; Meetsma, A.; Feringa, B. L. *Org. Biomol. Chem.* **2008**, *6*, 507−512.

(3) (a) Stoddart, J. F. *Acc. Chem. Res.* **2001**, *34*, 410−411. (b) Kottas, G. S.; Clarke, L. I.; Horinek, D.; Michl, J. *Chem. Rev.* **2005**, *105*, 1281−1376. (c) Irie, M. *Bull. Chem. Soc. Jpn.* **2008**, *81*, 917−926. (d) Balzani, V.; Credi, A.; Venturi, M. *Chem. Soc. Rev.* **2009**, *38*, 1542−1550.

(4) (a) Pollard, M. M.; Lubomska, M.; Rudolf, P.; Feringa, B. L. *Angwew. Chem., Int. Ed.* **2007**, *46*, 1278−1280. (b) London, G.; Carroll, G. T.; Fernández Landaluce, T.; Pollard, M. M.; Rudolf, P.; Feringa, B. L. *Chem. Commun.* **2009**, 1712−1714. (c) Browne, W. R.; Feringa, B. L. *Annu. Rev. Phys. Chem.* **2009**, *60*, 407−428. (d) London, G.; Chen, K.-Y.; Carroll, G. T.; Feringa, B. L. *Chem.—Eur. J.* **2013**, *19*, 10690−10697. (e) Ogino, S.; Kawamoto, M.; Okano, K.; Yamashita, T. J. *Photopolymer Sci. Technol.* **2013**, *26*, 563−566.

(5) Kudernac, T.; Ruangsupapichat, N.; Parschau, M.; Macia, B.; Katsonis, N.; Harutyunyan, S. R.; Ernst, K.-H.; Feringa, B. L. *Nature* **2011**, *479*, 208−211.

(6) Wang, J.; Feringa, B. L. *Science* **2011**, *331*, 1429−1432.

(7) Kazaryan, A.; Kistemaker, J. C. M.; Schäfer, L. V.; Browne, W. R.; Feringa, B. L.; Filatov, M. *J. Phys. Chem. A* **2010**, *114*, 5058−5067.

(8) Kazaryan, A.; Lan, Z.; Schäfer, L. V.; Thiel, W.; Filatov, M. *J. Chem. Theory Comput.* **2011**, *7*, 2189−2199.

(9) Conyard, J.; Addison, K.; Heisler, I. A.; Cnossen, A.; Browne, W. R.; Feringa, B. L.; Meech, S. R. *Nat. Chem.* **2012**, *4*, 547−551.

(10) Yarkony, D. R. *Rev. Mod. Phys.* **1996**, *68*, 985−1013.

(11) Bernardi, F.; Olivucci, M.; Robb, M. A. *Chem. Soc. Rev.* **1996**, *25*, 321−328.

(12) Migani, A.; Olivucci, M. In *Conical Intersections. Electronic Structure, Dynamics and Spectroscopy*; Domcke, W., Yarkony, D. R., Köppel, H., Eds.; Advanced Series in Physical Chemistry; World Scientific: Singapore, 2004; Vol. *15*; pp 271−320.

(13) Levine, B. G.; Martínez, T. J. *Annu. Rev. Phys. Chem.* **2007**, *58*, 613−634.

(14) Robb, M. A. In *Conical Intersections. Theory, Computation and Experiment*; Domcke, W., Yarkony, D. R., Köppel, H., Eds.; Advanced Series in Physical Chemistry; World Scientific: Singapore, 2011; Vol. *17*; pp 3−50.

(15) Filatov, M. *WIREs: Comput. Mol. Sci.* **2013**, *3*, 427−437.

(16) Huix-Rotllant, M.; Filatov, M.; Gozem, S.; Schapiro, I.; Olivucci, M.; Ferré, N. *J. Chem. Theory Comput.* **2013**, *9*, 3917−3932.

(17) Filatov, M. *J. Chem. Theory Comput.* **2013**, *9*, 4526−4541.

(18) Teller, E. *J. Phys. Chem.* **1937**, *41*, 109−116.

(19) Herzberg, G.; Longuet-Higgins, H. C. *Discuss. Faraday Soc.* **1963**, *35*, 77−82.

(20) Longuet-Higgins, H. C. *Proc. R. Soc. London Ser. A* **1975**, *344*, 147−156.

(21) Atchity, G. J.; Xantheas, S. S.; Ruedenberg, K. *J. Chem. Phys.* **1991**, *95*, 1862−1876.

(22) Yarkony, D. R. In *Conical Intersections. Electronic Structure, Dynamics and Spectroscopy*; Domcke, W., Yarkony, D. R., Köppel, H., Eds.; Advanced Series in Physical Chemistry; World Scientific: Singapore, 2004; Vol. *15*; pp 41−127.

(23) Paterson, M. J.; Bearpark, M. J.; Robb, M. A.; Blancafort, L. *J. Chem. Phys.* **2004**, *121*, 11562−11571.

(24) Bonačić-Koutecký, V.; Koutecký, J.; Michl, J. *Angew. Chem., Int. Ed.* **1987**, *26*, 170−189.

(25) Haas, Y.; Cogan, S.; Zilberg, S. *Int. J. Quantum Chem.* **2005**, *102*, 961−970.

(26) Malhado, J. P.; Hynes, J. T. *J. Chem. Phys.* **2012**, *137*, 22A543.

(27) Salem, L.; Rowland, C. *Angew. Chem., Int. Ed.* **1972**, *11*, 92−111.

(28) Sauers, R. R. *Tetrahedron* **1999**, *55*, 10013−10026.

(29) Gozem, S.; Huntress, M.; Schapiro, I.; Lindh, R.; Granovsky, A. A.; Angeli, C.; Olivucci, M. *J. Chem. Theory Comput.* **2012**, *8*, 4069−4080.

(30) Gozem, S.; Schapiro, I.; Ferré, N.; Olivucci, M. *Science* **2012**, *337*, 1225−1228.

(31) Levine, B.; Coe, J. D.; Martínez, T. J. *J. Phys. Chem. B* **2008**, *112*, 405−413.

(32) Keal, T. W.; Wanko, M.; Thiel, W. *Theor. Chem. Acc.* **2008**, *123*, 145−156.

(33) Ohmine, I. *J. Chem. Phys.* **1985**, *83*, 2348−2362.

(34) Ben-Nun, M.; Martínez, T. J. *Chem. Phys.* **2000**, *259*, 237−248.

(35) Quenneville, J.; Martínez, T. J. *J. Phys. Chem. A* **2003**, *107*, 829−837.

(36) Virshup, A. M.; Chen, J.; Martínez, T. J. *J. Chem. Phys.* **2012**, *137*, 22A519.

(37) Mori, T.; Martínez, T. J. *J. Chem. Theory Comput.* **2013**, *9*, 1155−1163.

(38) Ioffe, I. N.; Granovsky, A. A. *J. Chem. Theory Comput.* **2013**, *9*, 4973−4990.

(39) Léonard, J.; Schapiro, I.; Briand, J.; Fusi, S.; Paccani, R. R.; Olivucci, M.; Haacke, S. *Chem.—Eur. J.* **2012**, *18*, 15296−15304.

(40) Lumento, F.; Zanirato, V.; Fusi, S.; Busi, E.; Latterini, L.; Elisei, F.; Sinicropi, A.; Andruniów, T.; Ferré, N.; Basosi, R.; Olivucci, M. *Angew. Chem., Int. Ed.* **2007**, *46*, 414−420.

(41) Sinicropi, A.; et al. *Proc. Nat. Acad. Sci. U.S.A.* **2008**, *105*, 17642−17647.

(42) Briand, J.; Bram, O.; Rehault, J.; Léonard, J.; Cannizzo, A.; Chergui, M.; Zanirato, V.; Olivucci, M.; Helbing, J.; Haacke, S. *Phys. Chem. Chem. Phys.* **2010**, *12*, 3178−3187.

(43) Dunkelberger, A. D.; Kieda, R. D.; Shin, J. Y.; Rossi Paccani, R.; Fusi, S.; Olivucci, M.; Fleming Crim, F. *J. Phys. Chem. A* **2012**, *116*, 3527−3533.

(44) (a) Polanyi, J. C. *Acc. Chem. Res.* **1972**, *5*, 161−168. (b) Polanyi, J. C. *Science* **1987**, *236*, 680−690.

(45) Shavitt, I. In *Modern Theoretical Chemistry Vol. 3: Methods of Electronic Structure Theory*; Schaefer, H. F., III, Ed.; Plenum: New York, 1977; pp 189−275.

(46) (a) Roos, B. O. In *Ab Initio Methods in Quantum Chemistry II*; Lawley, K. P., Ed.; John Wiley and Sons: New York, 1987; pp 399−446. (b) Andersson, K.; Malmqvist, P.; Roos, B. O. *J. Chem. Phys.* **1992**, *96*, 1218−1226.

(47) Filatov, M.; Shaik, S. *Chem. Phys. Lett.* **1999**, *304*, 429−437.

(48) Filatov, M.; Shaik, S. *J. Phys. Chem. A* **2000**, *104*, 6628−6636.

(49) Moreira, I. d. P. R.; Costa, R.; Filatov, M.; Illas, F. *J. Chem. Theory Comput.* **2007**, *3*, 764−774.

(50) Lieb, E. H. *Int. J. Quantum Chem.* **1983**, *24*, 243−277.

(51) (a) Englisch, H.; Englisch, R. *Phys. Status Solidi B* **1984**, *123*, 711−721. (b) Englisch, H.; Englisch, R. *Phys. Status Solidi B* **1984**, *124*, 373−379.

(52) Schipper, P. R. T.; Gritsenko, O. V.; Baerends, E.-J. *Theor. Chem. Acc.* **1998**, *99*, 329−343.

(53) Schipper, P. R. T.; Gritsenko, O. V.; Baerends, E.-J. *J. Chem. Phys.* **1999**, *111*, 4056−4067.
(54) Ullrich, C. A.; Kohn, W. *Phys. Rev. Lett.* **2001**, *87*, 093001.
(55) Morrison, R. C. *J. Chem. Phys.* **2002**, *117*, 10506−10511.
(56) Giesbertz, K. J. H.; Baerends, E.-J. *J. Chem. Phys.* **2010**, *132*, 194108.
(57) Ziegler, T.; Rauk, A.; Baerends, E. J. *Theor. Chim. Acta* **1977**, *43*, 261−271.
(58) Filatov, M.; Shaik, S. *Chem. Phys. Lett.* **1998**, *288*, 689−697.
(59) Filatov, M.; Shaik, S. *J. Chem. Phys.* **1999**, *110*, 116−125.
(60) (a) Gaudoin, R.; Burke, K. *Phys. Rev. Lett.* **2004**, *93*, 173001. (b) Gaudoin, R.; Burke, K. *Phys. Rev. Lett.* **2005**, *94*, 029901.
(61) (a) Schautz, F.; Buda, F.; Filippi, C. *J. Chem. Phys.* **2004**, *121*, 5836−5844. (b) Filippi, C.; Buda, F. *J. Chem. Phys.* **2005**, *122*, 087102.
(62) (a) Gross, E. K. U.; Oliveira, L. N.; Kohn, W. *Phys. Rev. A* **1988**, *37*, 2805−2808. (b) Gross, E. K. U.; Oliveira, L. N.; Kohn, W. *Phys. Rev. A* **1988**, *37*, 2809−2820. (c) Oliveira, L. N.; Gross, E. K. U.; Kohn, W. *Phys. Rev. A* **1988**, *37*, 2821−2833.
(63) Kazaryan, A.; Heuver, J.; Filatov, M. *J. Phys. Chem. A* **2008**, *112*, 12980−12988.
(64) Kraka, E.; Filatov, M.; Zou, W.; Gräfenstein, J.; Izotov, D.; Gauss, J.; He, Y.; Wu, A.; Polo, V.; Olsson, L.; Konkoli, Z.; He, Z.; Cremer, D. COLOGNE2012. 2012.
(65) Krishnan, R.; Binkley, J. S.; Seeger, R.; Pople, J. A. *J. Chem. Phys.* **1980**, *72*, 650−654.
(66) Becke, A. D. *J. Chem. Phys.* **1993**, *98*, 1372−1377.